



Research paper

Efficient ultrafast energy-down-shift upon ultraviolet excitation in methylammonium lead bromide nanoplatelets

Xingzhi Wang, Shengyuan Wang, Wei Pan^{*}, Wenzhong Shen^{*}

Laboratory of Condensed Matter Spectroscopy and Opto-Electronic Physics, and Key Laboratory of Artificial Structures and Quantum Control (Ministry of Education), School of Physics and Astronomy, Shanghai Jiao Tong University, Shanghai 200240, China



ARTICLE INFO

Keywords:

MAPbBr₃ NPLs
Mixed-phase
Photoluminescence
Efficient energy transfer

ABSTRACT

Methylammonium lead bromide (MAPbBr₃) nanocrystals have attracted great attention for potential optoelectronic applications. We synthesized highly emissive MAPbBr₃ nanoplatelets (NPLs) by using a facile ligand assisted reprecipitation method with short-chain ligands. They exhibit an excitation-dependent photoluminescence (PL) quantum yield (QY) with a maximum value of 98% upon ultraviolet (UV) excitation. The femtosecond transient absorption and temperature-dependent PL spectra confirmed the existence of continuous band at ~350 nm and demonstrated that the PLQY of near unity originates from the efficient ultrafast energy-down-shift from this band to exciton state in N phase, which quenches nonradiative recombination via trap states.

Solution processed quasi-two dimensional (2D) lead halide perovskites have become a promising class of material for optoelectronic applications such as light emitting devices and solar cells due to their flexible and controllable structures, tunable and excellent optoelectronic properties, and ease of synthesis [1–5]. Lots of efforts have been paid on the fabrication of quasi-2D perovskites with high photoluminescence (PL) quantum yield (QY) to serve as light emitting materials [6–11]. Among them, methylammonium lead bromide (MAPbBr₃) is one of the mostly studied quasi-2D perovskites. Compared to silicon, MAPbBr₃ has a relatively strong absorption in ultraviolet (UV)-blue shortwave length region [12]. Simultaneously, MAPbBr₃ also exhibit higher PLQY (>90%) when irradiated with UV light [7,13]. Therefore, it is highlighted as luminescent down-shifting layer in luminescent solar concentrators and solar cells, and also as emitters in light emitting diodes [14,15].

Recent studies have demonstrated that rapid reorganization makes quasi-2D perovskites prepared at room temperature generally possess a collection of phases with different layer thickness *n* even though with stoichiometry-controlled precursors for a specific thickness [14,16,17]. Different phase distribution would affect charge transport and device performance. Hence, a compressive understanding of photophysics in mixed phase systems is advantaged to better utilizing them in diverse optoelectronic applications. However, to date, researches about photophysics in quasi-2D MAPbBr₃ focus on the carrier dynamics upon excitation ranging from blue to near infrared [18–20]. Seldom effort has

been paid on those with UV-blue excitation, which is crucial to device applications, especially down-conversion luminescent devices.

Herein, we report the efficient ultrafast energy-down-shift process in mixed-phase MAPbBr₃ nanoplatelets (NPLs) upon UV excitation. Structural and optical characterization demonstrate these mixed-phase MAPbBr₃ possess excitation-dependent PLQY. Femtosecond (fs) transient absorption (TA) spectra illustrate the influence of pump energy on the energy transfer routings and energy-down-shift rates from excited-to emissive- states. It confirms that efficient ultrafast energy-down-shift from continuous band produces a PLQY of near unity upon UV excitation. Temperature-dependent PL further demonstrates the quenching of nonradiative recombination via trap states at room temperature. This work reports the ultrafast energy-down-shift process upon UV excitation in quasi-2D MAPbBr₃ and provides a comprehensive understanding of their carrier dynamics.

The highly emissive perovskite NPLs were fabricated by a facile ligand assisted reprecipitation (LARP) method with a modification by replacing long-chain ligands with short-chain phenethylamine (PEA) and acetic acid (HAc) [21]. The modified protocol is also suitable for the one-step synthesis of colloidal MAPb(Br_{1-x}Cl_x)₃ (*x* = 0 ~ 0.43) NPLs (Fig. S1) and solid-state MAPbBr₃ NPLs thin films (Fig. S2). The detailed description about fabrication and characterization is given in supplementary material. Transmission electron microscopy (TEM) image in Fig. 1a shows that these square-shaped MAPbBr₃ NPLs possess an

^{*} Corresponding authors.

E-mail addresses: sjtushelwill@sjtu.edu.cn (W. Pan), wzshen@sjtu.edu.cn (W. Shen).

average lateral size of 43 ± 11 nm (Fig. S3). X-ray diffraction (XRD) pattern in Fig. 1b displays two series of diffraction peaks, a series of strong peaks (red solid circles) at 5.41° , 10.76° , 16.09° , 21.49° , 26.91° , and 32.40° , and another series of tiny peaks (blue solid circles) at 15.11° and 30.34° . As shown in inset of Fig. 1b, the strong and tiny peaks correspond to the lattice spacing of 16.54 \AA (d_1 , strong peaks) and 5.88 \AA (d_N , tiny ones). d_N agrees well with the lattice constant of cubic-phase bulk MAPbBr_3 [22,23], while d_1 is in consistency with the thickness of single PbBr_6^{4-} octahedral layer covered by phenethylamine [24,25]. Obviously, XRD pattern indicates the coexistence of NPLs with single and multiple layers. Atomic force microscopy (AFM) image in Fig. 1c and the cross section diagram in Fig. 1d demonstrate that the square-shaped NPLs have a typical thickness of ~ 4 nm and a lateral size of ~ 60 nm (consistent with TEM observation). Further statistical analysis in Fig. 1e indicates an average thickness of NPLs is 5.2 ± 1.3 nm, much larger than that (16.54 \AA) of NPLs with single PbBr_6^{4-} octahedral layer. XRD and AFM results indicate the existence of NPLs with single ($n = 1$) and multiple layers ($n = N$) stacking within a single NPL, similar to previous reports [14,26]. Consequently, exciton states of single and multiple layers are possible to exist in a single mixed-phase NPL.

UV-visible (vis) absorption spectrum of NPLs dispersed in toluene in

Fig. 1f displays an obvious absorption peak at ~ 515 nm and a tiny absorption peak at ~ 411 nm, corresponding to exciton absorption in $n = N$ ($\bar{N} \approx 8$) and 1 phase [24,27]. PL spectrum in Fig. 1f further displays a dominant green emission centered at 529 nm with a full width at half maximum (FWHM) of 22 nm, which can be assigned to radiative exciton recombination in $n = N$ phase [28]. Meanwhile, no emission is observed at ~ 411 nm, implying exciton energy in $n = 1$ phase is possibly transferred via nonradiative routings. Similar PL behaviors are observed in Fig. S4 with different excitations. The excitation-independent emission centered at 529 nm indicates main emission indeed originates from radiative recombination of excitons confined in $n = N$ phase. Absolute PLQY measurement in Fig. S5 shows a value of 93.5% (colloidal NPLs solution in toluene) at excitation of 350 nm. The excitation-dependent PLQY in Fig. 1g displays a U-shaped variation over the range of 320 \sim 530 nm. The PLQY with excitations near emissive state (ES, exciton state in N phase) energy is calculated by decomposing spectra into absorption and emission peaks with two-peak Gaussian fitting (Fig. S6). High PLQY achieved at 530 nm illustrates less trap states lying below ES. The abrupt decrease at 520 nm indicates trap states are mainly distributed a little higher than ES, suggesting the nature of shallow traps [29,30]. The sudden enhancement at short wavelengths implies the

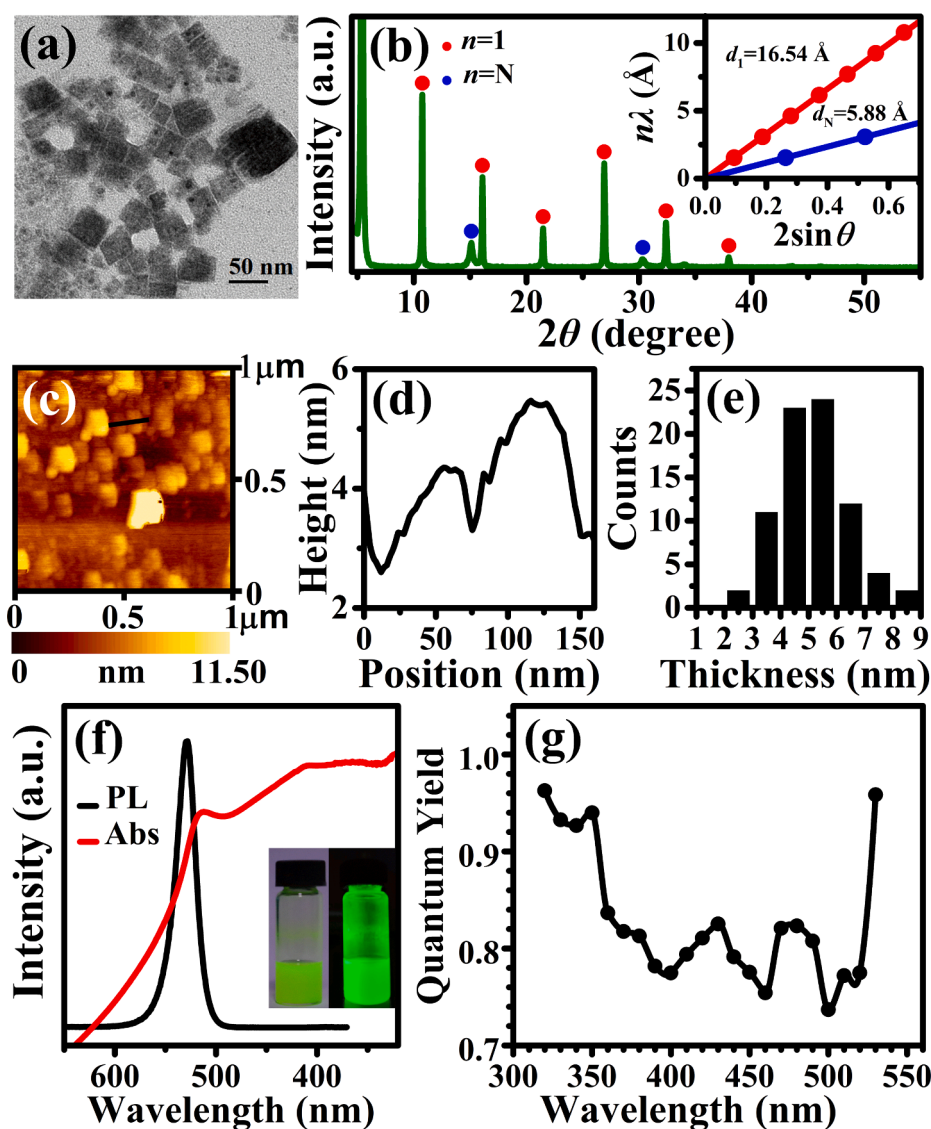


Fig. 1. (a) TEM image; (b) XRD spectrum; (c) AFM image; (d) Height profile; (e) Height distribution; (f) UV-vis absorption (abs, red) and PL (at 350 nm excitation, black) spectra of MAPbBr_3 NPLs. The inset of Fig. 1(f) is the digital photograph under daylight and UV illumination. (g) PLQYs of MAPbBr_3 NPLs with different excitations.

existence of energy level at ~ 350 nm, which possibly possess an ultrafast charge transfer to ES. The shallow trap possibly come from Br vacancies (V_{Br}) since the mixed-phase NPLs were synthesized in a Br-deficient atmosphere. Control experiments demonstrate that Br-rich synthesis by using PEA and hydrobromic acid leads to the simultaneous formation of blue-light and green-light emitting NPLs (Fig. S7) while using only PEA as ligands results in the rapid aggregation of NPLs and extremely low PLQY (11%, Fig. S8), implying the contribution of HAC to reaction kinetics and colloidal stability [31]. The high-resolution Pb 4f x-ray photoelectron spectroscopy (XPS) spectrum in Fig. S9 reflects the existence of Pb-Br and Pb-acetate, suggesting the imperfect lattice structure due to V_{Br} .

To explore the carrier dynamics behaviours, fs-TA spectra were measured at different pump energies. Fig. 2 and Fig. S10 display fs-TA spectra of colloidal MAPbBr₃ NPLs pumped at 350 nm (Fig. 2a-c), 400 nm (Fig. 2d-f) and 300 nm (Fig. S10) with a fluence of 84 $\mu\text{J}/\text{cm}^2$, corresponding to an average photons number absorbed in a single NPL $\langle N \rangle \approx 4.5$ and average carrier density per NPL volume $\langle n \rangle \approx 5 \times 10^{17} \text{ cm}^{-3}$. The carrier density $\langle n \rangle$ and average photon number $\langle N \rangle$ were evaluated from absorbance and pump intensity via method reported previously, [32] whose details are illustrated in the supplementary information. TA spectra pumped at 350 nm (Fig. 2a) and 300 nm (Fig. S10) display three distinct photoinduced bleaching (PB) features at ~ 350 nm (CB_2), ~ 400 nm (PB_1), and ~ 515 nm (PB_N). PB_1 and PB_N correspond to the filling of exciton states in $n = 1$ (PB_1) and N (PB_N) phases. The PB at ~ 350 nm denoted by CB_2 is probably from Pb-6p related step-like continuous band (3.3 \sim 3.5 eV) at the same point as quasi-continuous band (CB_1) in the Brillouin zone [23,33], which has been observed in PbBr-based perovskites, such as bulk MAPbBr₃ and monolayer NPLs [34,35]. The strong photoinduced absorption (PA) observed before 2 ps is probably induced by the exciton-exciton interactions [18]. When pumped at 350 nm (Fig. 2b-c), electrons were firstly excited to CB_2 and then relaxed to exciton states in different phases to build up PB_1 and PB_N . TA kinetics in Fig. 2c show that both PB_1 and PB_N appear at ~ 0.2

ps, indicating excitons in both $n = 1$ and N phases originate from CB_2 . However, as shown in Fig. 2d-f, when pumped at 400 nm, TA spectra exhibit an extra PB at ~ 453 nm (PB_3) and different hot carrier relaxation process. Upon 400 nm excitation, PB_1 appears instantaneously, implying excitons are directly generated in $n = 1$ phase. Following the ultrafast buildup, parts of photogenerated excitons transfer to $n = 3$ phase, resulting in a rapid establishment of PB_3 (Fig. 2d). After that, parts of hot carriers travel through nonradiative channel to ground states. The remaining carriers transfer to N phase, leading to the rapid rise of PB_N . TA kinetics further demonstrate that the rise of PB_N seems to be well matched with the decay of PB_1 and PB_3 , suggesting the transfer from $n = 1$ and 3 phase to N phase. Consequently, at the excitation of 400 nm, energy in small- n phases is transferred to large- n phase sequentially, similar to previous reports in 2D perovskites [8,36], but different from those excited with UV light. Meanwhile, TA spectra in Fig. S11–13 excited by low intensities also display the different relaxation path induced by pump energy. Excitons created by 300 nm excitation with an intensity of $\langle N \rangle = 0.13$, relax to continuous band and also exciton states in $n = 1$ and N phase (Fig. S11). When pumped at 350 nm with low intensities [$\langle N \rangle = 0.42$ and 2.1], hot carriers directly transfer to exciton states in N phase (Fig. S12). However, excitons created by 400 nm pump [$\langle N \rangle = 0.45$ and 2.3] relax to exciton states both in $n = 3$ and N phase rapidly, resulting in the fast buildup of PB_3 and PB_N (Fig. S13).

To further reveal the ongoing photoinduced hot carrier relaxation process, global analysis [37] were applied on TA spectra. Fig. 3a-b and Fig. S14 display the decay associate spectra (DAS) with low excitation intensities [$\langle N \rangle \approx 0.16, 0.4$, and 2] at 400 and 350 nm, respectively. Most of TA spectra were decomposed into three kinetics components. The slow component (>3 ns) associated with PB_N was assigned to exciton radiative recombination, whose lifetime is on the timescale of ns (Fig. S15). The ultrafast component (<1 ps) with negative amplitude ranging from 430 to 506 nm was attributed to hot carrier cooling, which increases with pump intensity due to hot phonon bottleneck effect. [38] The middle component (tens of ps) displays a negative amplitude

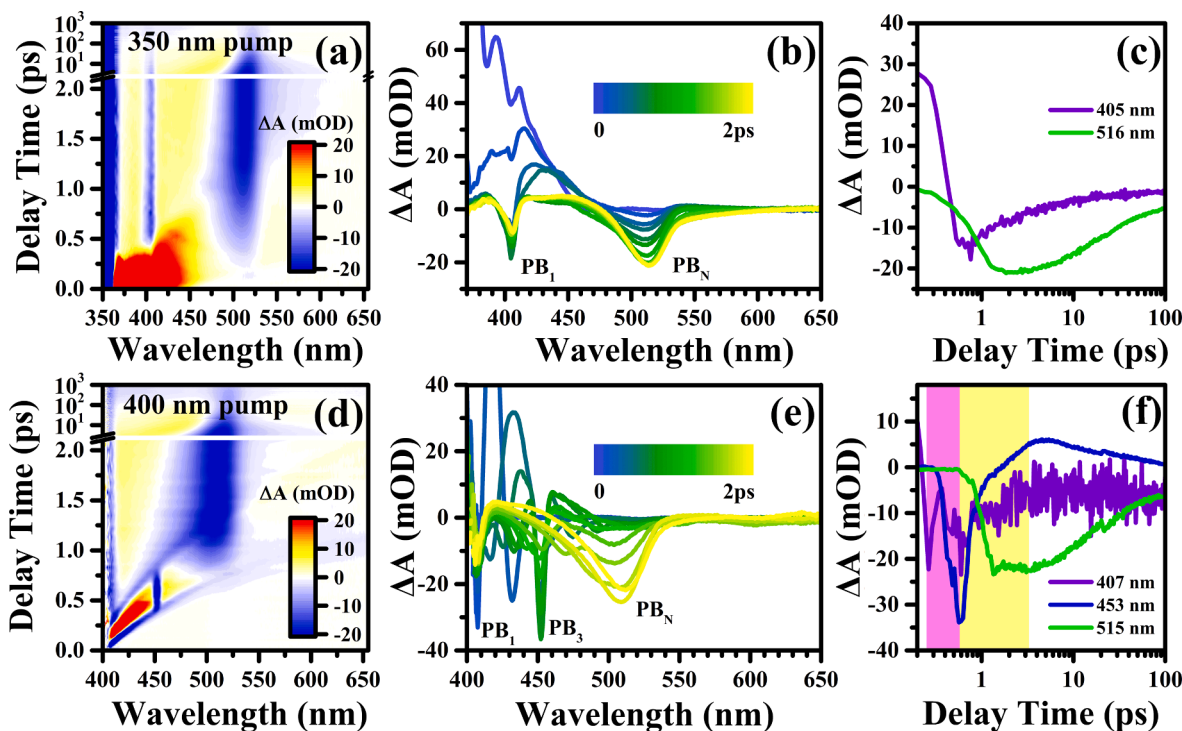


Fig. 2. (a) TA map as a function of probe photon energy and pump-probe delay after 350 nm excitation. (b) TA spectra of MAPbBr₃ NPLs probed at different delay times extracted from (a). (c) Decay dynamics of exciton states in $n = 1$ and N phase extracted from (a). (d) TA map as a function of probe photon energy and pump-probe delay after 400 nm excitation. (e) TA spectra of MAPbBr₃ NPLs probed at different delay times extracted from (d). (f) Decay dynamics of exciton states in $n = 1, 3$, and N phase extracted from (d).

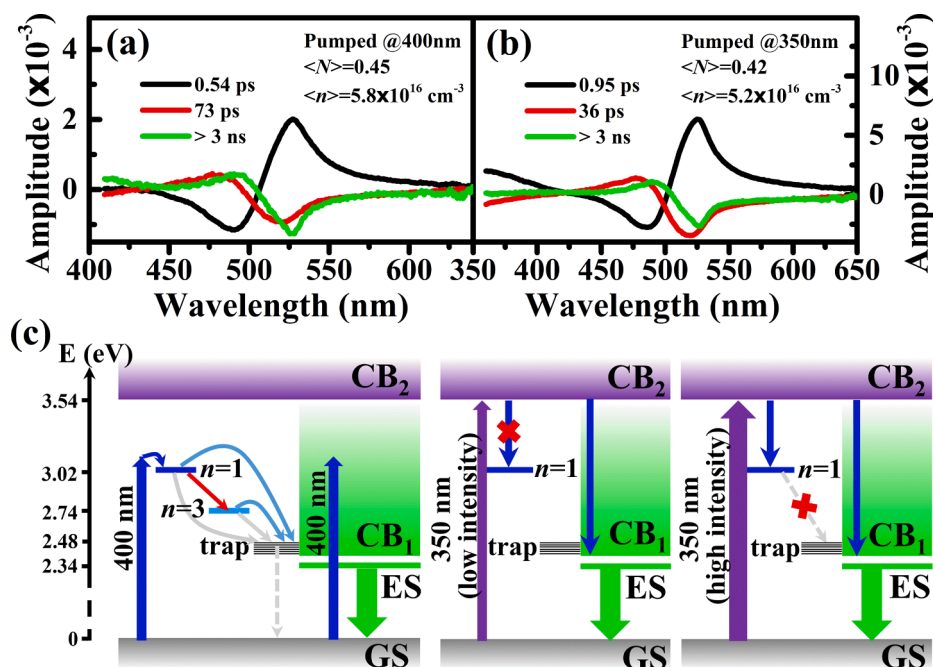


Fig. 3. Decay associated spectra of MAPbBr₃ NPLs under the excitation of (a) 400 and (b) 350 nm. (c) Schematics of the band diagrams and illustration of photophysical processes excited by 400 (left) and 350 nm with low (middle) and high intensity (right).

centered at ~ 515 nm, which is probably related to band filling effect. Notably, when pumped at 400 nm with an intensity of $\langle N \rangle = 0.17$, DAS spectra did not show this middle component, implying the weakening of band filling effect under low excitation intensity. Furthermore, for both 350 and 400 nm pump, time constant of middle component becomes faster with increasing excitation intensity, indicating the enhanced carrier-carrier interactions induced by more hot carriers relaxing to band edge [39]. On the other hand, when pumped by same fluence, the time constants of middle component decomposed from TA spectra under 350 excitation are shorter than those under 400 excitation, suggesting that more hot carriers relaxing to band edge when pumped at 350 nm. Because the minimums of CB₁ and CB₂ are at the same point in Brillouin zone [23,33], hot carrier cooling process is very likely to be direct transition, faster and more efficient than that under 400 nm excitation, which is a phonon-assisted indirect transition process. Fig. 3c displays the schematic of energy band diagram, which summarizes above discussion about physical process in mixed-phase NPL. When pumped at 400 nm (left), carriers are excited to exciton state in $n = 1$ phase (blue line) and CB₁ (green square) in $n = N$ phase. The carriers in $n = 1$ phase

then transfer to CB₁. After that, hot carriers in CB₁ relax to band edge (blue arrows). During the transfer process from small- n to large- n phases, carriers are possibly captured by shallow traps (black lines) lying above ES and lose their energy through nonradiative recombination, leading to the decreasing PLQY. Upon UV excitation, with low intensity (middle), electrons excited to CB₂ transfer into CB₁ rapidly, and then directly to band edge (violet arrows) and ES. If pumped with higher intensity (right), few electrons relaxed to exciton state in $n = 1$ phase. It could explain two local minimums of PLQY at 400 and 460 nm, and the sudden enhancement at 350 nm in excitation-dependent PLQYs shown in Fig. 1g. In addition, under the excitation of 350 nm, it seems that the nonradiative routing to shallow traps via exciton state in $n = 1$ phase is suppressed, which needs to be further verified by the aid of temperature dependent PL.

To perform the temperature-dependent (83 ~ 303 K) PL spectra, NPLs were incorporated into polymethyl methacrylate matrix to form the composite films. The composite film exhibits PL emission centered at ~ 534 nm with a PLQY of 77% (Fig. S12a), and two decay constants of 7.9 and 64.6 ns (Fig. S12b). Fig. 4a shows temperature-dependent (83 ~ 303 K) PL spectra of NPLs thin film on silicon substrate excited by 325 nm laser. Obviously, as observed in lead composite semiconductors [40], PL peak continuously blueshifts with increasing temperature, which is possibly due to lattice expansion with a positive expansion coefficient [41]. PL intensity in Fig. 4b shows a rapid decrease and then a slow enhancement with the increasing temperature. The rapid decrease of PL intensity at 83 ~ 203 K exhibits typical thermal quenching caused by thermal dissociation of excitons at higher temperatures, which is usually described as $I(T) = I_0/[1 + C \exp(-E_b/k_B T)]$ with E_b of exciton binding energy. The best fitting curve (blue dash line) yields an exciton binding energy of 67 ± 1 meV, basically consistent with those reported values (65 ~ 76 meV) in bulk MAPbBr₃ [31,34,42]. The abnormal increase of PL intensity at 200 ~ 300 K indicates other competitive mechanisms play a dominant role, such as delocalization/capture of carriers by the trap/intermediate states. Therefore, another term considering the activation of carriers at trap/intermediate states must be added. As discussed above, shallow trap states and intermediate states such as exciton state in $n = 1$ phase, locate above ES, so that carriers are possibly recaptured by trap/intermediate states before

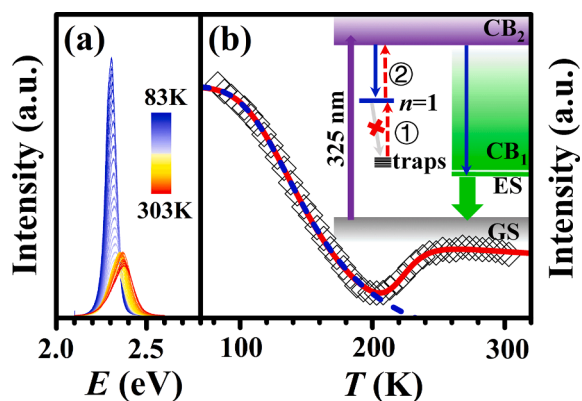


Fig. 4. (a) PL spectra of MAPbBr₃ NPLs at different temperatures. (b) Temperature-dependent PL intensity. The inset of (b) is the energy-level diagram.

relaxed to ES in $n = N$ phase. Here, a model based on delocalization and recapture of carriers is used to explain the temperature-dependent intensity $I(T)$, described as [43,44]:

$$I(T) = I_0 \frac{1 + D_1 \exp(-E_2/k_B T)}{1 + C_1 \exp(-E_b/k_B T) + C_2 \exp(-E_1/k_B T)} \quad (1)$$

where E_b is exciton binding energy of 67 meV obtained above, E_1 and E_2 describes the activation energy for process that facilitate nonradiative and radiative recombination, respectively. A good agreement between experimental data (hollow diamond) and best-fit curve (red solid line) gives $E_1 = 530 \pm 39$ meV and $E_2 = 523 \pm 51$ meV, respectively. Previous discussion in Fig. 3c has demonstrated that energy difference between exciton state in $n = 1$ phase and CB_2 , and that from exciton state in $n = 1$ phase and trap states are ~ 500 meV, in good agreement with activation energies E_1 and E_2 . Consequently, there are two possible activation approaches. The carriers localized in trap states are activated into the exciton state in $n = 1$ phase, or/and those in exciton state in $n = 1$ phase are excited into the CB_2 . Both of them suppress carrier transfer from CB_2 to $n = 1$ phase, and facilitate the transfer routing from CB_2 to $n = N$ phase, in consistence with TA observation. Therefore, we attribute the enhancement of integrated PL at 200 \sim 300 K to the quenching of nonradiative recombination via exciton state in $n = 1$ phase, which is usually benefit to nonradiative recombination.[45] Moreover, the variation curve of line width with temperature in Fig. S13 also displays a knee point at ~ 200 K. The slowing trend of broadening suggests the sudden weakening of electron-phonon interaction since linewidth broadening is mainly from the electron-phonon interaction [46,47]. This abrupt change of electron-phonon interaction possibly originates from the reorientation of organic cations or functional groups, which weakening the electron-phonon interaction [48].

In conclusion, we have synthesized highly emissive MAPbBr₃ NPLs by using facile and fast LARP method with short-chain ligands. These NPLs exhibit excitation-dependent PLQYs, which reach near unity when excited with UV light. TA spectra further demonstrate the different carrier transfer process induced by pumped energy and the existence of Pb-6p related step-like CB_2 in all phases of NPLs. The efficient ultrafast energy-down-shift from this band to ES is the key to realize a PLQY of near unity upon UV excitation. Temperature-dependent PL spectra further demonstrates the quenching of nonradiative recombination at room temperature. This work provides a detailed research on the carrier dynamics in mixed-phase quasi-2D MAPbBr₃ systems upon UV excitation, and is instructive to improve the performance of perovskite-based optoelectronic devices.

See supplementary material for the detailed synthesis and characterization of studied MAPbBr₃ NPLs.

CRedit authorship contribution statement

Kingzhi Wang: Conceptualization, Investigation, Validation, Formal analysis, Writing - original draft, Data curation, Visualization. **Shengyuan Wang:** Investigation, Validation. **Wei Pan:** Conceptualization, Methodology, Formal analysis, Supervision, Visualization. **Wenzhong Shen:** Supervision, Project administration, Funding acquisition.

Declaration of Competing Interest

The authors declare that they have no known competing financial interests or personal relationships that could have appeared to influence the work reported in this paper.

Acknowledgement

This work was supported by Natural Science Foundation of China (11834011) and Shanghai Science and Technology Commission (19XD1402100).

Appendix A. Supplementary data

Supplementary data to this article can be found online at <https://doi.org/10.1016/j.cplett.2020.138192>.

References

- [1] Y. Chen, Y. Sun, J. Peng, J. Tang, K. Zheng, Z. Lian, Adv. Mater. 30 (2018) 1703487.
- [2] Y. Zheng, T. Niu, X. Ran, J. Qiu, B. Li, Y. Xia, Y. Chen, W. Huang, J. Mater. Chem. A 7 (2019) 13860.
- [3] Y. Jiang, J. Yuan, Y. Ni, J. Yang, Y. Wang, T. Jiu, M. Yuan, J. Chen, Joule 2 (2018) 1356.
- [4] M.C. Weidman, A.J. Goodman, W.A. Tisdale, Chem. Mater. 29 (2017) 5019.
- [5] J. Wang, J. Dong, F. Lu, C. Sun, Q. Zhang, N. Wang, J. Mater. Chem. A 7 (2019) 23563.
- [6] Z. Yuan, Y. Shu, Y. Xin, B. Ma, Chem. Commun. 52 (2016) 3887.
- [7] S. Dai, B. Hsu, C. Chen, C. Lee, H. Liu, H. Wang, Y. Huang, T. Wu, A. Manikandan, R. Ho, C. Tsao, C. Cheng, Y. Chueh, H. Lin, Adv. Mater. 30 (2018) 1705532.
- [8] Y. Shang, G. Li, W. Liu, Z. Ning, Adv. Funct. Mater. 28 (2018) 1801193.
- [9] X. Yang, X. Zhang, J. Deng, Z. Chu, Q. Jiang, J. Meng, P. Wang, L. Zhang, Z. Yin, J. You, Nat. Commun. 9 (2018) 570.
- [10] S. Yang, W. Niu, A.L. Wang, Z. Fan, B. Chen, C. Tan, Q. Lu, H. Zhang, Angew. Chem. Int. Ed. 56 (2017) 4252.
- [11] J. Chang, S. Zhang, N. Wang, Y. Sun, Y. Wei, R. Li, C. Yi, J. Wang, W. Huang, J. Phys. Chem. Lett. 9 (2018) 881.
- [12] K.A. Bush, A.F. Palmstrom, Z.J. Yu, M. Boccard, R. Cheacharoen, J.P. Mailoa, D. P. McMeekin, R.L.Z. Hoyer, C.D. Bailie, T. Leijtens, I.M. Peters, M.C. Minichetti, N. Rolston, R. Prasanna, S. Sofia, D. Harwood, W. Ma, F. Moghadam, H.J. Snaith, T. Buonassisi, Z.C. Holman, S.F. Bent, M.D. McGehee, Nat. Energy 2 (2017) 17009.
- [13] Y. Wu, C. Wei, X. Li, Y. Li, S. Qiu, W. Shen, B. Cai, Z. Sun, D. Yang, Z. Deng, H. Zeng, ACS Energy Letters 3 (2018) 2030.
- [14] M. Wei, F.P.G. de Arquer, G. Walters, Z. Yang, L.N. Quan, Y. Kim, R. Sabatini, R. Quintero-Bermudez, L. Gao, J.Z. Fan, F. Fan, A. Gold-Parker, M.F. Toney, E. H. Sargent, Nature Energy 4 (2019) 197.
- [15] L. Meng, X.G. Wu, S. Ma, L. Shi, M. Zhang, L. Wang, Y. Chen, Q. Chen, H. Zhong, Nanophotonics 9 (2020) 93.
- [16] X. Zhang, R. Munir, Z. Xu, Y. Liu, H. Tsai, W. Nie, J. Li, T. Niu, D.M. Smilgies, M. G. Kanatzidis, A.D. Mohite, K. Zhao, A. Amassian, S.F. Liu, Adv. Mater. 30 (2018) 1707166.
- [17] L. Kuai, J. Li, Y. Li, Y. Wang, P. Li, Y. Qin, T. Song, Y. Yang, Z. Chen, X. Gao, B. Sun, ACS Energy Letters 5 (2020) 8.
- [18] K. Wei, T. Jiang, Z. Xu, J. Zhou, J. You, Y. Tang, H. Li, R. Chen, X. Zheng, S. Wang, K. Yin, Z. Wang, J. Wang and X. Cheng, Laser Photonics Rev. 12, 1800128 (2018).
- [19] L.N. Quan, Y. Zhao, F.P. Garcia de Arquer, R. Sabatini, G. Walters, O. Voznyy, R. Comin, Y. Li, J.Z. Fan, H. Tan, J. Pan, M. Yuan, O.M. Bakr, Z. Lu, D.H. Kim, E. H. Sargent, Nano Lett. 17 (2017) 3701.
- [20] M. Yuan, L.N. Quan, R. Comin, G. Walters, R. Sabatini, O. Voznyy, S. Hoogland, Y. Zhao, E.M. Beauregard, P. Kanjanaboos, Z. Lu, D.H. Kim, E.H. Sargent, Nat. Nanotechnol. 11 (2016) 872.
- [21] A. Pan, B. He, X. Fan, Z. Liu, J.J. Urban, A.P. Alivisatos, L. He, Y. Liu, ACS Nano 10 (2016) 7943.
- [22] J. Dai, H. Zheng, C. Zhu, J. Lu, C. Xu, J. Mater. Chem. C 4 (2016) 4408.
- [23] C. Chen, X. Hu, W. Lu, S. Chang, L. Shi, L. Li, H. Zhong, J.B. Han, J. Phys. D: Appl. Phys. 51 (2018), 045105.
- [24] N. Kitazawa, Y. Watanabe, J. Phys. Chem. Solids 71 (2010) 797.
- [25] S. Yuan, Z.K. Wang, L.X. Xiao, C.F. Zhang, S.Y. Yang, B.B. Chen, H.T. Ge, Q.S. Tian, Y. Jin, L.S. Liao, Adv. Mater. 31 (2019) 1904319.
- [26] Q. Shang, Y. Wang, Y. Zhong, Y. Mi, L. Qin, Y. Zhao, X. Qiu, X. Liu, Q. Zhang, J. Phys. Chem. Lett. 8 (2017) 4431.
- [27] S. Kashiwamura, N. Kitazawa, Synthetic Met. 96 (1998) 133.
- [28] Q. Wang, X.D. Liu, Y.H. Qiu, K. Chen, L. Zhou, Q.Q. Wang, AIP Advances 8 (2018), 025108.
- [29] N. Mondal, A. Samanta, Nanoscale 9 (2017) 1878.
- [30] S. Park, H. Cho, W. Choi, H. Zou, D.Y. Jeon, Nanoscale Adv. 1 (2019) 2828.
- [31] F. Zhang, H.Z. Zhong, C. Chen, X.G. Wu, X.M. Hu, H.L. Huang, J.B. Han, B.S. Zou, Y.P. Dong, ACS Nano 9 (2015) 4533.
- [32] J. Yang, X. Wen, H. Xia, R. Sheng, Q. Ma, J. Kim, P. Tapping, T. Harada, T.W. Kee, F. Huang, Y. Cheng, M. Green, A.H. Baillie, S. Huang, S. Shrestha, R. Patterson, G. Conibeer, Nat. Commun. 8 (2017) 14120.
- [33] N. Kitazawa, M. Aono, Y. Watanabe, Thin Solid Films 518 (2010) 3199.
- [34] K. Tanaka, T. Takahashi, T. Ban, T. Kondo, K. Uchida, N. Miura, Solid State Commun. 127 (2003) 619.
- [35] K. Tanaka, T. Takahashi, T. Kondo, K. Umeda, K. Ema, T. Umabayashi, K. Asai, K. Uchida, N. Miura, Jpn. J. Appl. Phys. 44 (2005) 5923.
- [36] P. Li, C. Liang, X.L. Liu, F. Li, Y. Zhang, X.T. Liu, H. Gu, X. Hu, G. Xing, X. Tao, Y. Song, Adv. Mater. 31 (2019) 1901966.
- [37] X. Jiang, S. Jun, J. Hoffman, M.G. Kanatzidis, E. Harel, J. Phys. Chem. A 124 (2020) 4837.
- [38] Y. Yang, D.P. Ostrowski, R.M. France, K. Zhu, J. Lagemaat, J.M. Luther, M. C. Beard, Nat. Photon. 10 (2016) 53.
- [39] T. Kim, S. Jung, S. Ham, H. Chung, D. Kim, Small 15 (2019) 1900355.
- [40] Z. M. Gibbs, H. Kim, H. Wang, R. L. White, F. Drymiotis, M. Kaviani, and G. Jeffrey Snyder, Appl. Phys. Lett. 103, 262109 (2013).

- [41] Q. Wei, X. Li, C. Liang, Z. Zhang, J. Guo, G. Hong, G. Xing, W. Huang, *Adv. Opt. Mater.* 7 (2019) 1900080.
- [42] S. Rana, K. Awasthi, S.S. Bhosale, E.W.G. Diau, N. Ohta, *J. Phys. Chem. C* 123 (2019) 19927.
- [43] H. Shibata, *Jpn. J. Appl. Phys.* 37 (1998) 550–553.
- [44] J. Li, L. Luo, H. Huang, C. Ma, Z. Ye, J. Zeng, H. He, *J. Phys. Chem. Lett.* 8 (2017) 1161.
- [45] T. Wu, Y. Yang, Y. Zou, Y. Wang, C. Wu, Y. Han, T. Song, Q. Zhang, X. Gao, B. Sun, *Nanoscale* 10 (2018) 19322.
- [46] A.D. Wright, C. Verdi, R.L. Milot, G.E. Eperon, M.A. Perez-Osorio, H.J. Snaith, F. Giustino, M.B. Johnston, L.M. Herz, *Nat. Commun.* 7 (2016) 11755.
- [47] R. Saran, A. Heuer-Jungemann, A.G. Kanaras, R.J. Curry, *Adv. Opt. Mater.* 5 (2017) 1700231.
- [48] H. Zhu, K. Miyata, Y. Fu, J. Wang, P.P. Joshi, D. Niesner, K.W. Williams, S. Jin, X. Y. Zhu, *Science* 353 (2016) 1409.